International Journal of Minerals, Metallurgy and Materials
Volume 25, Number 11, November 2018, Page 1329
https://doi.org/10.1007/s12613-018-1686-4

Structural and electrical properties of HCl–polyaniline–Ag composites synthesized by polymerization using Ag-coated $(NH_4)_2S_2O_8$ powder

You Zhou, Yu-he Zhang, Jun-sheng Ma, Ming-peng Yu, and Hong Qiu

School of Mathematics and Physics, University of Science and Technology Beijing, Beijing 100083, China

(Received: 3 January 2018; revised: 18 June 2018; accepted: 19 June 2018)

Abstract: Ag nanoparticles were sputter-deposited on ammonium persulfate ($(NH_4)_2S_2O_8$) powder to obtain $(NH_4)_2S_2O_8$–Ag powder, which was used to synthesize the HCl-doped polyaniline–Ag (HCl–PANI–Ag) composite via a polymerization procedure. The Ag nanoparticles were dispersed in the HCl–PANI matrix, and their sizes mainly ranged from 3 to 6 nm. The Ag nanoparticles did not affect the structure of emeraldine salt in the composite, and they increased the ordered crystalline regions in the HCl–PANI matrix. The HCl–PANI–Ag composite had a conductivity of (6.8 ± 0.1) S/cm, which is about four times larger than that of the HCl–PANI. The charge transport mechanism in the composite is explained by the three-dimensional Mott variable-range hopping (3D-Mott-VRH).

Keywords: hydrochloric-acid-doped polyaniline; silver nanoparticles; composite; structure; conductivity

1. Introduction

Composites with polyaniline (PANI) and Ag nanoparticles have attracted scientific interests because of their potential applications. Syntheses of the PANI–Ag composites have been achieved by chemical methods, in which the Ag nanoparticles were prepared by silver nitrate ($AgNO_3$) solutions. Khanna *et al.* [1] prepared PANI–Ag nanocomposites by reducing Ag salt in aniline. Kang *et al.* [2] used polyvinylpyrrodione-stabilized and aniline-stabilized Ag colloids to synthesize PANI–Ag nanocomposites. Oliveira *et al.* [3] used dodecanethiol-stabilized Ag nanoparticles to obtain PANI–Ag nanocomposites by a two-phase water/toluene interfacial reaction. Jing *et al.* [4] synthesized PANI–Ag nanocomposites via a chemical oxidation polymerization of aniline based on a mercaptocarboxylic acid-capped Ag nanoparticle colloid. Lee *et al.* [5] synthesized PANI–Ag composite particles via a two-step reaction process comprising PANI reduction by the substitution of 3-mercapto-1,2-propanediol (MPD) and a redox reaction between $AgNO_3$ and MPD-substituted PANI. Bouazza *et al.* [6] prepared a PANI–Ag composite by reducing Ag ions with PANI in $AgNO_3$ aqueous solution. Stejskal's group [7–12] carried out a series of detailed studies on the synthesis of the PANI–Ag nanocomposites, which include (1) aniline oxidation with $AgNO_3$ in solutions of nitric acid, (2) $AgNO_3$ reduction with various PANI salts, (3) aniline oxidation with $AgNO_3$ in sulfonic acids solutions, (4) aniline oxidation with mixed oxidants, $AgNO_3$, and ammonium peroxydisulfate, (5) aniline oxidation with Ag ions and the reduction of Ag ions with PANI. Roussel *et al.* [13] used $AgNO_3$ to chemically synthesize PANI–Ag composites having a silver volume fraction of 2% to 34%. Huang *et al.* [14] used different oxidation states of PANI and $AgNO_3$ to prepare PANI–Ag composites by a one-step synthesis method. Besides, we sputter-deposited Ni and Fe nanoparticles on HCl-doped PANI (HCl–PANI) pellets. Then, these pellets were mechanically milled to obtain HCl–PANI–Ni and HCl–PANI–Fe composites [15–16]. The sputter-deposition is a physical preparation method; thus, studies are being carried out to determine the possibility of sputter-depositing Ag nanoparticles on solid chemicals to synthesize HCl–PANI–Ag composites, which is of great scientific and practical significance. Therefore, in this study, Ag nanoparticles were deposited on ammonium persulfate ($(NH_4)_2S_2O_8$) powder by direct-current sputtering. Then the $(NH_4)_2S_2O_8$–Ag powder

Corresponding author: Hong Qiu E-mail: qiuhong@sas.ustb.edu.cn

was used to synthesize HCl–PANI–Ag composite via a polymerization procedure. The structural properties of the composites were analyzed using transmission electron microscopy (TEM), X-ray diffraction (XRD), and Fourier transform infrared spectroscopy (FT-IR). The composite conductivity is measured by a four-point probe technique, and the temperature dependence of the conductivity is measured from 100 to 290 K.

2. Experimental

Analytically pure reagents and chemicals were purchased from Beijing Chemical Works. The aniline was doubly distilled under reduced pressure and stored at 4°C. Ag nanoparticles were deposited on $(NH_4)_2S_2O_8$ powder at room temperature by an SBC-12 sputtering system (KYKY Technology Co., Ltd.) [17–18]. The Ag target had a diameter of 60 mm and purity of 99.99%. The $(NH_4)_2S_2O_8$ powder weighed 4.929 g. It was evenly divided into four sets, and every part was sputter-coated with Ag nanoparticles to obtain an $(NH_4)_2S_2O_8$–Ag powder. Each set of the $(NH_4)_2S_2O_8$ powder was evenly spread in a tray (2 cm × 4 cm) and placed in a sputter-deposition chamber. The distance between the target and the tray was 40 mm. Prior to deposition, the chamber was evacuated to 2 Pa for 2 min by a rotary pump. The sputtering conditions were an Ar gas (99.9995% pure) pressure of 4 Pa, a voltage of 1000 V, and a current of 6 mA. The Ag deposition rate was 13 nm/min, and the total deposition time was 60 s. To maintain a room-temperature deposition of Ag, the 60-s deposition was divided into six stages, where the deposition time of each stage was 10 s, and there was an interval of 15 s between two subsequent depositions. The Ag nanoparticles had a bulk density of 10.53 g/cm^3, and the Ag content in the $(NH_4)_2S_2O_8$–Ag powder was about 0.009wt%.

By substituting the pure $(NH_4)_2S_2O_8$ powder with $(NH_4)_2S_2O_8$–Ag powder, HCl–PANI–Ag composite was synthesized via the well-established polymerization procedure [15–16,19]. The raw HCl–PANI–Ag powder consisted of some small agglomerate particles; therefore, it was mechanically milled at the constant speed in an agate mortar for 30 min in ambient conditions to obtain a fine and uniform HCl–PANI–Ag composite powder. For comparison, pure HCl–PANI was also synthesized by the same procedure.

The structure of the Ag nanoparticles in the composite was observed using TEM (F20, Philips), and the structures of the composite and HCl–PANI were analyzed by XRD (Rigaku) under the standard θ–2θ scan using Cu K_α radiation (wavelength λ = 0.15406 nm). The molecular structures of the composite and HCl–PANI were analyzed by FT-IR (Nexus). The HCl–PANI–Ag composite and HCl–PANI powders were pressed at the same pressure into pellets with a thickness of 0.5 mm and diameter of 13 mm. The room-temperature resistances R of the pellets were measured by the four-point probe technique. The conductivity σ of the pellet is given by the following equation [15–16]:

$$\sigma = \frac{1}{3.31 \times R \times d} \tag{1}$$

where 3.31 × R is the sheet resistance, and d is the pellet thickness measured by a micrometer. The room-temperature conductivities of three HCl–PANI–Ag pellets and three HCl–PANI pellets were measured, and the average was taken as the final conductivity. The conductivities of HCl–PANI–Ag composite and HCl–PANI were measured within 100–290 K using the CFM-5T-H3-CFVTI-1.6K-24.5 system (Cryogenic).

3. Results and discussion

Fig. 1 shows a TEM microphotograph and high-resolution TEM (HRTEM) images of the HCl–PANI–Ag composite.

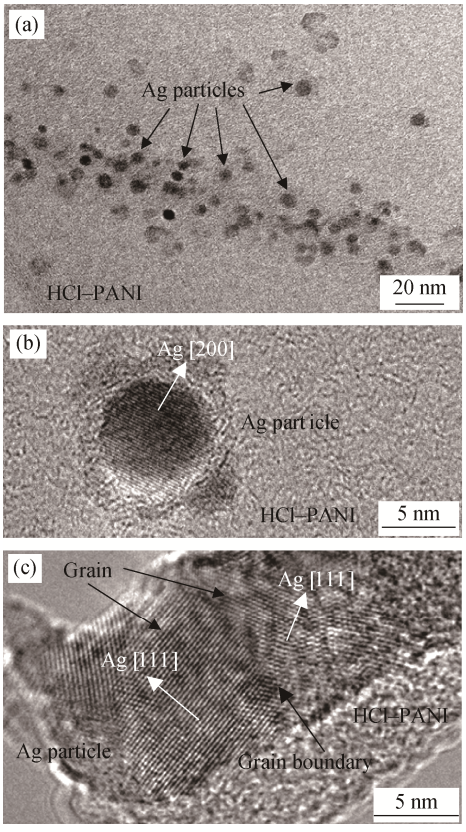

Fig. 1. TEM (a) and HRTEM (b, c) microphotographs of the HCl-PANI-Ag composite.

Ag nanoparticles, including aggregates, were present in the composite (Fig. 1(a)). According to the HRTEM images (Figs. 1(b) and 1(c)), the Ag (200) and Ag (111) plane spacings were calculated to be (0.209 ± 0.002) nm and (0.238 ± 0.001) nm, respectively. On the basis of the Ag (200) and Ag (111) plane spacings, the average lattice constant of Ag nanoparticles was (0.414 ± 0.002) nm, which is a little larger than that of the bulk Ag (0.4086 nm). It is considered that some impurity atoms such as C, N, and O were present in the Ag nanoparticles when they were sputter-deposited on the $(NH_4)_2S_2O_8$ powder. Furthermore, the grain boundary between the Ag nanoparticles was narrow. A distribution of the Ag nanoparticle size in the composite can be obtained from Fig. 1(a). Fig. 2 shows the Ag nanoparticle size distribution, which was narrow and mainly ranged from 3 to 6 nm.

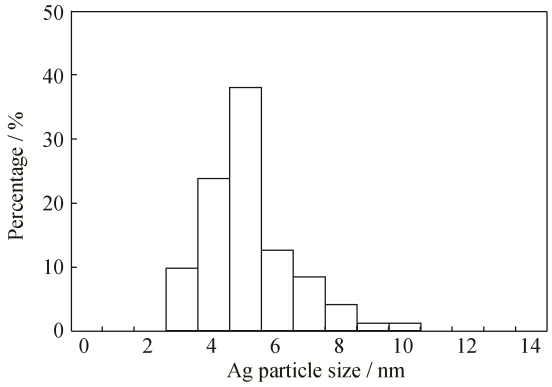

Fig. 2. Ag nanoparticle size distribution in the HCl–PANI–Ag composite.

The XRD patterns of the HCl–PANI and the HCl–PANI–Ag composite (Fig. 3) show that they had an emeraldine salt structure (ES-I) [20–21]. The Ag nanoparticles did not affect the emeraldine salt structure in the composite. Furthermore, the Ag diffraction peaks cannot be observed because the amount of Ag nanoparticles was too small to be detected by XRD. However, the diffraction peaks of the HCl–PANI–Ag composite were stronger than those of the HCl–PANI. This indicates that the polymer chains in the composite were more ordered than those in the HCl–PANI; i.e., the composite had more ordered crystalline regions than the HCl–PANI. The presence of Ag nanoparticles between polymer chains promotes the separation of chains and improves inter-chain stacking; therefore, the Ag nanoparticles enhanced the ordered alignment of the chains. The diffraction peak at about 25° corresponded to the *d*-spacing, which is related to the distance between the phenyl rings of adjacent chains, i.e., the periodicity perpendicular to the polymer chains [21–22]. The *d*-spacing of the HCl–PANI–Ag composite (0.354 nm) was slightly larger than that of the HCl–PANI (0.349 nm). This suggests that Ag nanoparticles existed between the polymer chains.

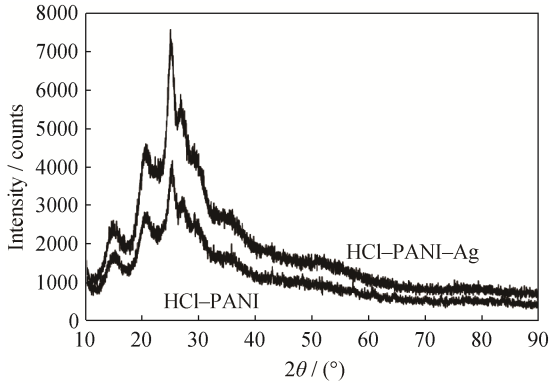

Fig. 3. XRD patterns of the HCl–PANI and the HCl–PANI–Ag composite.

The FT-IR spectra of the HCl–PANI and the HCl–PANI–Ag composite (Fig. 4) show that the two samples had the same absorption peak positions. The peaks at 1572 and 1468 cm^{-1} are related to the presence of a quinone structure and benzene ring stretching [23–24]; therefore, the aromatic structure of PANI was retained in the HCl–PANI–Ag composite. Furthermore, the peak intensity ratio between the 1572 and 1468 cm^{-1} peaks for the two samples was the

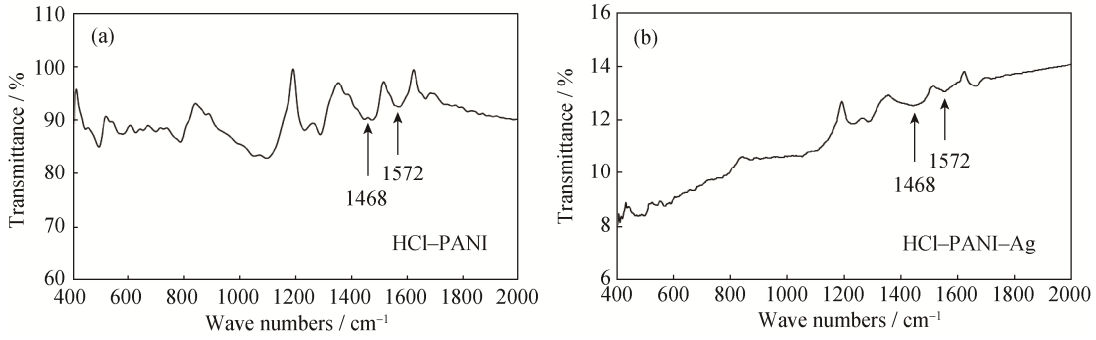

Fig. 4. FT-IR spectra of the HCl–PANI (a) and the HCl–PANI–Ag composite (b).

same, which indicates that the Ag nanoparticles did not change the oxidation state of PANI [23]. The HCl–PANI–Ag composite had a lower infrared transmittance compared with the HCl–PANI; this is attributed to scattering of the infrared light waves by the Ag nanoparticles in the composite.

The relationship between voltage V and current I for the HCl–PANI pellet and the HCl–PANI–Ag composite pellet (Fig. 5) reveals that the voltage linearly increased with current, indicating that the two samples exhibit ohmic characteristics. The slope of the straight line in Fig. 5 gives the resistance R of the pellet. The conductivities of the HCl–PANI and the HCl–PANI–Ag composite were calculated in terms of Eq. (1), where the former was (1.4 ± 0.1) S/cm and the latter was (6.8 ± 0.1) S/cm. The conductivity of the HCl–PANI–Ag composite was about four times larger than that of the HCl–PANI. In the composite, the Ag nanoparticles were dispersed in the HCl–PANI matrix. The content of Ag nanoparticles was little and did not reach the percolation threshold in the HCl–PANI matrix [10]. Therefore, the increase of conductivity for the composite is attributed to the Ag conductive junction between the HCl–PANI agglomerates [25] or between polymer chains and the electronic tunneling through the Ag nanoparticles [26]. Furthermore, the increase of the ordered crystalline region in the HCl–PANI–Ag composite can also lead to its higher conductivity compared to the HCl–PANI [27].

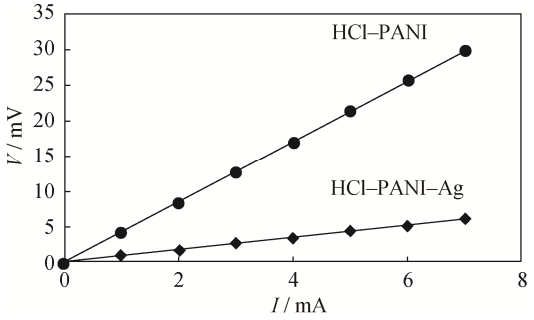

Fig. 5. Relationship between voltage V and current I for the HCl–PANI and the HCl–PANI–Ag composite.

Fig. 6 shows a temperature (T) dependence of the conductivity (σ) for the HCl–PANI and the HCl–PANI–Ag composite. For both samples, the conductivity increased with temperature (Fig. 6(a)). In the three-dimensional Mott variable-range-hopping (3D-Mott-VRH) model, a temperature T dependence of conductivity σ is given by [15–16,28]

$$\sigma = \sigma_0 \exp\left[-\left(\frac{T_0}{T}\right)^{\frac{1}{4}}\right] \tag{2}$$

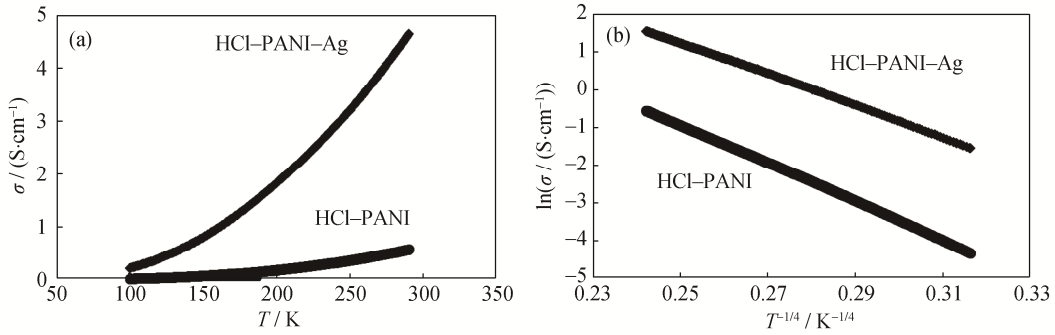

Fig. 6. Temperature (T) dependence of the conductivity (σ) for the HCl–PANI and the HCl–PANI–Ag composite: (a) σ versus T; (b) lnσ versus $T^{-1/4}$.

where T_0 is the Mott characteristic temperature, and σ_0 is the conductivity at $T = \infty$. T_0 is given by [29–30]

$$T_0 = \frac{18.1}{k \times N(E_F) \times L^3} \tag{3}$$

where k is the Boltzmann constant, $N(E_F)$ is the density of the localized states at Fermi level, and L is the localization length of the wave function in the localized state. The hopping distance R_{hop} and hopping energy W_{hop} are expressed as Eqs. (4) and (5), respectively [29–30].

$$R_{hop} = \left[\frac{9L}{8\pi \times k \times N(E_F) \times T}\right]^{\frac{1}{4}} \tag{4}$$

$$W_{hop} = \frac{3}{4\pi \times N(E_F) \times R_{hop}^3} \tag{5}$$

The temperature dependences of the HCl–PANI and the HCl–PANI–Ag composite conductivities, plotted as lnσ versus $T^{-1/4}$ (Fig. 6(b)), show that the two samples exhibited a good linear dependence in 100–290 K. The linear correlation coefficient was better than 0.9995, indicating that the 3D-Mott-VRH model can be used to explain the carrier transport mechanism in the HCl–PANI and the HCl–PANI–Ag composite. The T_0 value was obtained by the slope of the fitted line in Fig. 6(b), and L was assumed to be 0.3 nm, i.e., the width of aniline monomer unit [29–30].

Using Eq. (3), $N(E_F)$ was calculated. Then, using Eqs. (4) and (5), R_{hop} and W_{hop} at room temperature (300 K) were obtained, respectively. The values of T_0, $N(E_F)$, R_{hop}, and W_{hop} are summarized in Table 1. The HCl–PANI–Ag composite had a larger localized state density, shorter hopping distance, and lower hopping energy than the HCl–PANI (Table 1). The HCl–PANI consists of ordered conductive crystalline regions and disordered non-conductive amorphous regions, and the conductive crystalline region is surrounded by the non-conductive amorphous region. The electronic wave function is localized in the ordered crystalline region by the disordered amorphous region. The hopping conduction is caused by electron hopping from one crystalline region (localized state) to other crystalline region [27]. The Ag nanoparticles increased the ordered crystalline regions, as shown by the XRD results. Thus, the HCl–PANI–Ag composite had a larger localized state density, a shorter hopping distance, and a lower hopping energy compared with the HCl–PANI, indicating that the composite had larger carrier concentration and easier carrier migration compared with the HCl–PANI. Therefore, the conductivity of the HCl–PANI–Ag composite was larger than that of the HCl–PANI.

Table 1. Mott characteristic temperatures (T_0), localized state densities ($N(E_F)$), hopping distances (R_{hop}), and hopping energies (W_{hop}) of the HCl–PANI–Ag composite and HCl–PANI

Sample	T_0 / (10^6 K)	$N(E_F)$ / (10^{21} eV^{-1}·cm^{-3})	R_{hop} / nm	W_{hop} / meV
HCl–PANI–Ag	2.94	2.65	1.1	64
HCl–PANI	6.58	1.18	1.4	79

4. Conclusion

Ag nanoparticles were sputter-deposited on $(NH_4)_2S_2O_8$ powders, and the obtained $(NH_4)_2S_2O_8$–Ag powder was used to synthesize the HCl–PANI–Ag composite via a polymerization procedure. The Ag nanoparticles were dispersed in the HCl–PANI matrix. Their sizes mainly ranged from 3 to 6 nm, and they did not affect the emeraldine salt structure in the composite. The Ag nanoparticles increased the ordered crystalline regions in the HCl–PANI matrix. The conductivity of the HCl–PANI–Ag composite was about four times larger than that of the HCl–PANI. The charge transport mechanism in the composite was explained by the 3D-Mott-VRH model.

Acknowledgements

The authors appreciate Dr. Xin Gao of the Analysis Center of School of Materials Science and Technology, University of Science and Technology Beijing for supporting with TEM observations. This work was financially supported by the Fundamental Research Funds for the Central Universities of China (No. 8220).

References

[1] P.K. Khanna, N. Singh, S. Charan, and A.K. Viswanath, Synthesis of Ag/polyaniline nanocomposite via an *in situ* photo-redox mechanism, *Mater. Chem. Phys.*, 92(2005), No. 1, p. 214.

[2] Y.O. Kang, S.H. Choi, A. Gopalan, K.P. Lee, H.D. Kang, and Y.S. Song, Tuning of morphology of Ag nanoparticles in the Ag/polyaniline nanocomposites prepared by γ-ray irradiation, *J. Non-Cryst. Solids*, 352(2006), No. 5, p. 463.

[3] M.M. Oliveira, E.G. Castro, C.D. Canestraro, D. Zanchet, D. Ugarte, L.S. Roman, and A.J.G. Zarbin, A simple two-phase route to silver nanoparticles/polyaniline structures, *J. Phys. Chem. B*, 110(2006), No. 34, p. 17063.

[4] S.Y. Jing, S.X. Xing, L.X. Yu, Y. Wu, and C. Zhao, Synthesis and characterization of Ag/polyaniline core-shell nanocomposites based on silver nanoparticles colloid, *Mater. Lett.*, 61(2007), No. 13, p. 2794.

[5] Y.H. Lee, J.H. Park, Y.D. Jun, D.W. Kim, J.J. Lee, Y.C. Kim, and S.G. Oh, 3-Mercapto-1,2-propanediol-substituted polyaniline/Ag nanocomposites prepared by concurrent reduction and substitution chemistry, *Synth. Met.*, 158(2008), No. 3-4, p. 143.

[6] S. Bouazza, V. Alonzo, and D. Hauchard, Synthesis and characterization of Ag nanoparticles-polyaniline composite powder material, *Synth. Met.*, 159(2009), No. 15-16, p. 1612.

[7] N.V. Blinova, J. Stejskal, M. Trchová, I. Sapurina, and G. Ćirić-Marjanović, The oxidation of aniline with silver nitrate to polyaniline-silver composites, *Polymer*, 50(2009), No. 1, p. 50.

[8] J. Stejskal, M. Trchová, J. Kovářová, L. Brožová, and J. Prokeš, The reduction of silver nitrate with various polyaniline salts to polyaniline-silver composites, *React. Funct. Polym.*, 69(2009), No. 2, p. 86.

[9] P. Bober, M. Trchová, J. Prokeš, M. Varga, and J. Stejskal, Polyaniline-silver composites prepared by the oxidation of aniline with silver nitrate in solutions of sulfonic acids, *Electrochim. Acta*, 56(2011), No. 10, p. 3580.

[10] P. Bober, J. Stejskal, M. Trchová, and J. Prokeš, Polyaniline-silver composites prepared by the oxidation of aniline with mixed oxidants, silver nitrate and ammonium peroxydisulfate: The control of silver content, *Polymer*, 52(2011), No. 26, p. 5947.

[11] P. Bober, J. Stejskal, M. Trchová, and J. Prokeš, In-situ prepared polyaniline-silver composites: Single- and two-step strategies, *Electrochim. Acta*, 122(2014), p. 259.

[12] P. Bober, P. Humpoliček, T. Syrový, Z. Capákova, L. Syrová, J. Hromádková, and J. Stejskal, Biological properties of printable polyaniline and polyaniline-silver colloidal dispersions stabilized by gelatin, *Synth. Met.*, 232(2017), p. 52.

[13] F. Roussel, R.C.Y. King, M. Kuriakose, M. Depriester, A. Hadj-Sahraoui, C. Gors, A. Addad, and J.F. Brun, Electrical and thermal transport properties of polyaniline/silver composites and their use as thermoelectric materials, *Synth. Met.*, 199(2015), p. 196.

[14] S.M. Huang, J.Q. Xu, X. Tao, X. Chen, F. Zhu, Y. Wang, R.F. Jiang, and G.F. Ouyang, Fabrication of polyaniline/silver composite coating as a dual-functional platform for microextraction and matrix-free laser desorption/ionization, *Talanta* 172(2017), p. 155.

[15] R.C. Liu, H. Qiu, H. Li, H. Zong, and C.Y. Fang, Fabrication and characteristics of composite containing HCl-doped polyaniline and Ni nanoparticles, *Synth. Met.*, 160(2010), No. 23-24, p. 2404.

[16] R.C. Liu, H. Qiu, H. Zong, and C.Y. Fang, Fabrication and characterization of composite containing HCl-doped polyaniline and Fe nanoparticles, *J. Nanomater.*, 2012(2012), p. 674104.

[17] Y. Huang, H. Qiu, H. Qian, F.P. Wang, L.Q. Pan, P. Wu, Y. Tian, and X.L. Huang, Effect of annealing on the characteristics of Au/$Ni_{80}Fe_{20}$ and Au/$Ni_{30}Fe_{70}$ bilayer films grown on glass, *Thin Solid Films*, 472(2005), No. 1-2, p. 302.

[18] P. Wu, H. Qiu, Y.Q. Zhao, D.H. Jiang, B. Zhang, X.D. Zhao, X.L. Huang, L.Q. Pan, and Y. Tian, Characteristics of resistivity and structure of silver films deposited in low vacuum, *Phys. Exp.*, 27(2007), No. 3, p. 3.

[19] P.N. Adams, P.J. Laughlin, A.P. Monkman, and A.M. Kenwright, Low temperature synthesis of high molecular weight polyaniline, *Polymer*, 37(1996), No. 15, p. 3411.

[20] M.E. Jozefowicz, R. Laversanne, H.H.S. Javadi, A.J. Epstein, J.P. Pouget, X. Tang, and A.G. MacDiarmid, Multiple lattice phases and polaron-lattice-spinless-defect competition in polyaniline, *Phys. Rev. B*, 39(1989), No. 17, p. 12958.

[21] J.P. Pouget, M.E. Jozefowicz, A.J. Epstein, X. Tang, and A.G. MacDiarmid, X-ray structure of polyaniline, *Macromolecules*, 24(1991), No. 3, p. 779.

[22] C. Nath and A. Kumar, Fractal like charge transport in polyaniline nanostructures, *Phys. B*, 426(2013), p. 94.

[23] G.E. Asturias, A.G. MacDiarmid, R.P. McCall, and A.J. Epstein, The oxidation state of "emeraldine" base, *Synth. Met.*, 29(1989), No. 1, p. 157.

[24] J.S. Tang, X.B. Jin, B.C. Wang, and F.S. Wang, Infrared spectra of soluble polyaniline, *Synth. Met.*, 24(1988), No. 3, p. 231.

[25] T.D. Castillo-Castro, E. Larios-Rodriguez, Z. Molina-Arenas, M.M. Castillo-Ortega, and J. Tanori, Synthesis and characterization of metallic nanoparticles and their incorporation into electroconductive polymer composites, *Compos. Part A*, 38(2007), No. 1, p. 107.

[26] K. Gupta, P.C. Jana, and A.K. Meikap, Optical and electrical transport properties of polyaniline-silver nanocomposite, *Synth. Met.*, 160(2010), No. 13-14, p. 1566.

[27] H.B. Gu, J. Guo, X.R. Yan, H.G. Wei, X. Zhang, J.R. Liu, Y.D. Huang, S.Y. Wei, and Z.H. Guo, Electrical transport and magnetoresistance in advanced polyaniline nanostructures and nanocomposites, *Polymer*, 55(2014), No. 17, p. 4405.

[28] M. Ghosh, A. Barman, A. K. Meikap, S. K. De, and S. Chatterjee, Hopping transport in HCl doped conducting polyaniline, *Phys. Lett. A*, 260(1999), No. 1-2, p. 138.

[29] A.P. Singh, S.A. Kumar, A. Chandra, and S.K. Dhawan, Conduction mechanism in Polyaniline-flyash composite material for shielding against electromagnetic radiation in X-band & Ku band, *AIP Adv.*, 1(2011), No. 2, art. No. 022147.

[30] S.A. Kumar, A.P. Singh, P. Saini, F. Khatoon, and S.K. Dhawan, Synthesis, charge transport studies, and microwave shielding behavior of nanocomposites of polyaniline with Ti-doped γ-Fe_2O_3, *J. Mater. Sci.*, 47(2012), No. 5, p. 2461.